Electronic Supplementary Material (ESI) for CrystEngComm.

Supporting Information

Hydrogen-bonding tuned hydroxo-bridged tetra-copper $Cu_4(bipy)_4$-cluster supramolecular network to layer coordination polymer

Jian Zhang[a], Yang-Yang Chen[a], Chun-Hong Tan[a,*], Xiao Ma,[b,*] Xiao-Feng Wang[a,c,*] and Guangchuan Ou[d]

[a] School of Chemistry and Chemical Engineering, University of South China, Hengyang 421001, P. R. China;

[b] Jiangsu Key Laboratory of Advanced Catalytic Materials and Technology, Advanced Catalysis and Green Manufacturing Collaborative Innovation Center, School of Petrochemical Engineering, Changzhou University, Changzhou 213164, P. R. China;

[c] Hunan Key Laboratory for the Design and Application of Actinide Complexes, University of South China, Hengyang 421001, P. R. China;

[d] Department of Biology and Chemistry, Hunan University of Science and Engineering, Yongzhou 425199, P. R. China.

Table of Contents

Figure S3. Curie–Weiss fit (red solid line) of the inverse magnetic susceptibility $1/\chi_M$ for **1**

Materials and Instruments

Three benzenedicarboxylic acids (Adamas-beta®) were purchased from Adamas Reagent Co. Ltd (Shanghai, China). Other chemicals were commercially available and used as received without further purification.

The C, H and N elemental analyses were carried out with a Vario EL elemental analyzer. The ATR-FTIR spectra of the powders without KBr were collected in the range of 500-4000 cm^{-1} by a Thermo Nicolet 6700 spectrometer. Powder X-ray diffraction (PXRD) data were collected on a Rigaku D/max 2200 diffractometer with Cu-Kα radiation (λ = 1.5418 Å).

Table S1. Crystallographic data for complexes **1-3**.

Compound	**1**	**2**	**3**
Formula	$C_{56}H_{60}Cu_4N_8O_{20}$	$C_{56}H_{72}Cu_4N_8O_{26}$	$C_{28}H_{42}Cu_2N_4O_{16}$
Mr	1419.28	1527.37	817.73
Temp (K)	296	296	296
Cryst system	triclinic	monoclinic	monoclinic
Space group	$P\bar{1}$	$P2_1/c$	$P2_1/c$
a/Å	9.0471(7)	14.6945(17)	16.609(5)
b/Å	12.6873(9)	17.218(2)	16.984(5)
c/Å	13.3662(9)	25.968(3)	13.707(4)
α/°	89.490(3)	90	90
β/°	73.453(3)	94.777(4)	110.014(5)
γ/°	75.303(3)	90	90
V/Å^3	1419.24(18)	6547.4(13)	3633.0(18)
Z	1	4	4
D_c/g cm^{-3}	1.661	1.549	1.495
μ/mm^{-1}	1.565	1.369	1.245
F (000)	728	3152	1696
R(int)	0.0298	0.0932	0.0394
Total reflections	14891	179831	36818
Unique reflections	6522	15129	8317
$I > 2\sigma(I)$	4661	10407	7190
R_1	0.0321	0.0481	0.0753
wR_2	0.1016	0.1142	0.2668
S	1.004	1.042	1.156

Table S2. Selected bond distances (Å) and angles（°）for complexes **1-3**.

1		**2**				**3**	
Bond lengths							
Cu1-O1	1.9436(17)	Cu1-O1	1.922(2)	Cu2-O1W	2.246(2)	Cu1-O5	1.950(3)
Cu1-O2	1.9277(17)	Cu1-O2	1.954(2)	Cu3-O4	1.916(2)	Cu1-O1	2.408(3)
Cu1-N3	1.977(2)	Cu1-O3	2.312(2)	Cu3-O3	1.9547(19)	Cu1-N2	2.005(4)
Cu1-N4	2.027(2)	Cu1-N1	2.023(3)	Cu3-O2	2.270(2)	Cu1-N1	1.993(4)
Cu2-O2	1.9129(18)	Cu1-N2	1.990(3)	Cu3-N8	2.020(3)	Cu2-O4	1.943(3)
Cu2-O1	1.9586(17)	Cu2-O1	1.923(2)	Cu4-O4	1.929(2)	Cu2-O1	1.965(3)
Cu2-N1	1.993(2)	Cu2-O2	1.959(2)	Cu4-O3	1.980(2)	Cu2-O5	2.392(3)
Cu2-N2	2.012(2)	Cu2-N3	2.005(3)	Cu4-N6	2.021(3)	Cu2-N3	2.012(4)
Cu2-O1W	2.2437(19)	Cu2-N4	2.023(3)	Cu4-O6	2.203(2)	Cu2-N4	1.992(4)

1		**2**		**3**	
Bond angles					
O2-Cu1-O1	82.26(7)	O1-Cu1-O2	81.90(9)	O5-Cu1-N1	174.76(14)
O2-Cu1-N3	95.87(9)	O1-Cu1-N2	98.04(11)	N1-Cu1-N2	81.22(16)
O1-Cu1-N3	177.72(8)	O2-Cu1-N2	177.25(10)	O5-Cu1-O1	81.24(11)
O2-Cu1-N4	162.17(8)	N2-Cu1-N1	80.77(11)	N2-Cu1-O1	93.21(13)
O1-Cu1-N4	100.53(8)	N1-Cu1-O3	95.07(9)	N1-Cu1-O1	94.64(13)
N3-Cu1-N4	80.85(9)	O1-Cu2-O2	81.76(9)	O5-Cu1-N2	102.17(14)
O1-Cu1-O1	83.24(7)	O1-Cu2-N3	170.52(10)	O1-Cu2-N4	175.27(14)
O2-Cu2-O1	82.25(7)	O2-Cu2-N3	97.83(10)	N4-Cu2-N3	80.92(16)
O2-Cu2-N1	170.44(8)	N3-Cu2-N4	80.46(11)	O1-Cu2-O5	81.34(11)
O1-Cu2-N1	97.62(8)	O1-Cu2-O1W	93.79(9)	N4-Cu2-O5	100.09(13)
O2-Cu2-N2	95.37(8)	O4-Cu3-O3	83.38(8)	N3-Cu2-O5	96.50(12)
O1-Cu2-N2	156.68(8)	O4-Cu3-N7	97.05(10)		
		N7-Cu3-N8	80.76(10)		
		O3-Cu4-O6	98.36(8)		
		N5-Cu4-O6	102.23(9)		

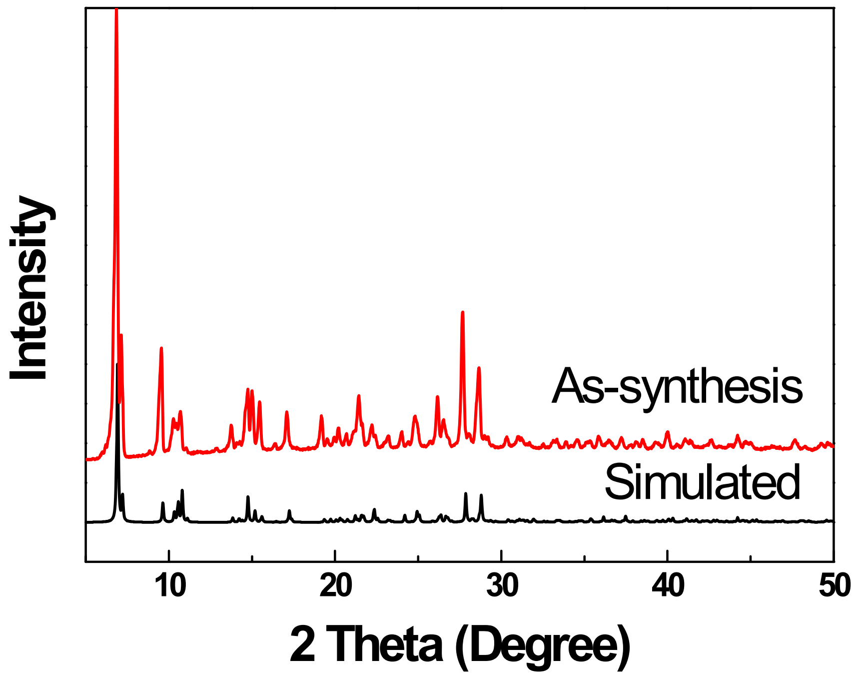

Figure S1. The PXRD curves of **1**.

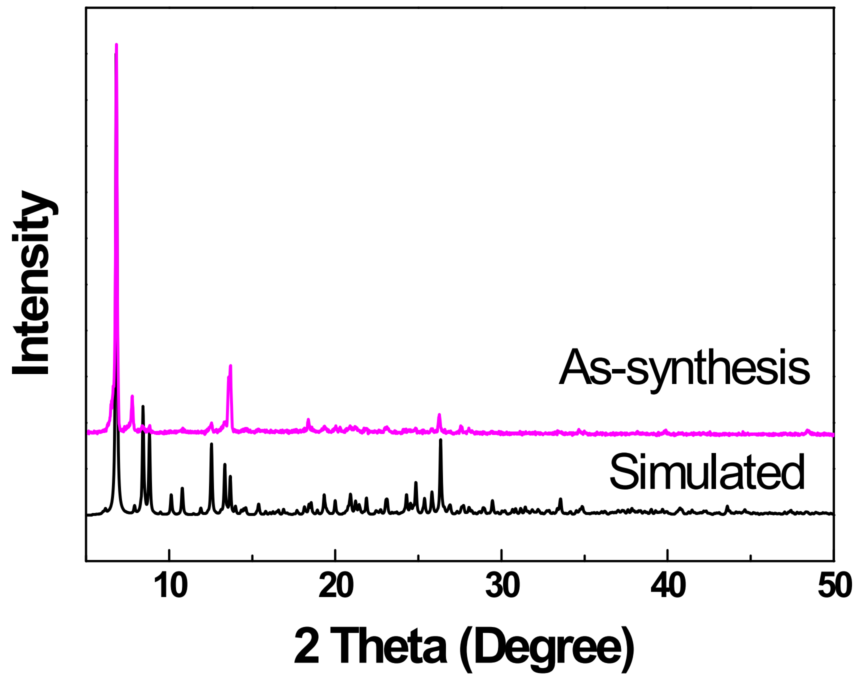

Figure S2. The PXRD curves of **2**.

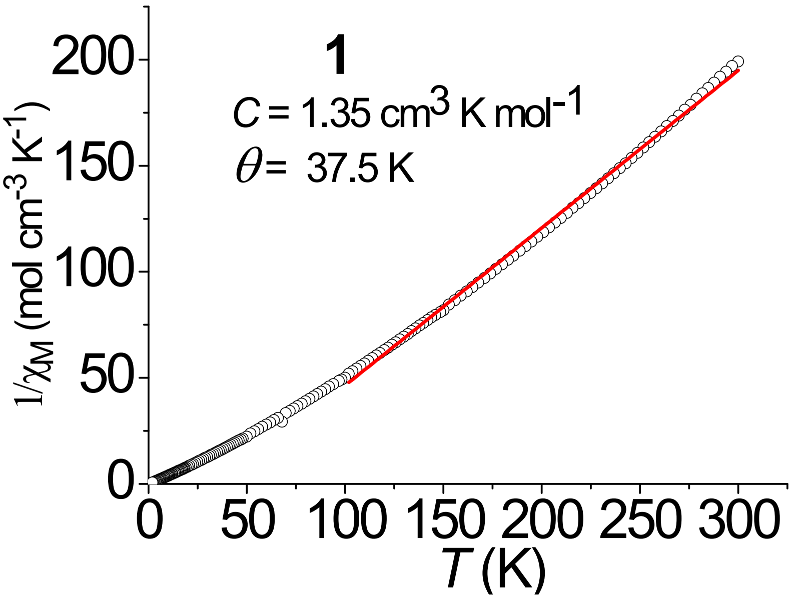

Figure S3. Curie–Weiss fit (red solid line) of the inverse magnetic susceptibility $1/\chi_M$ for **1**

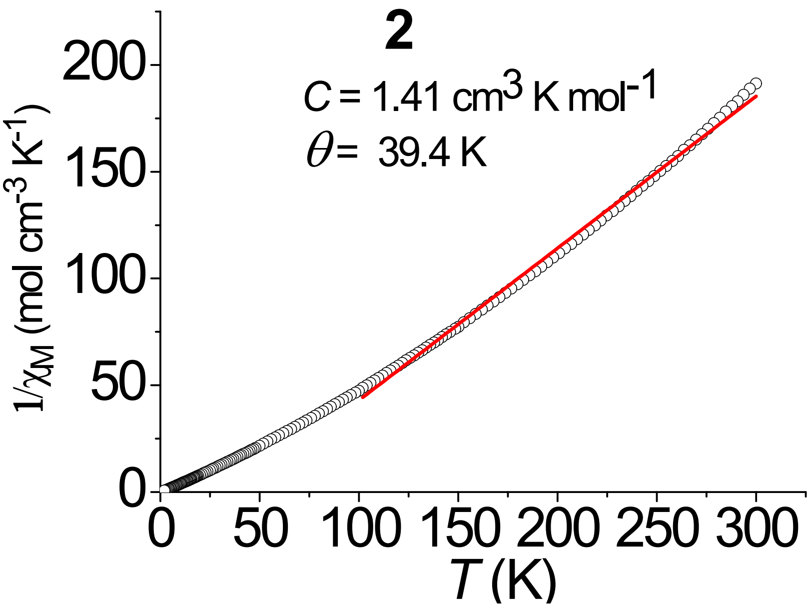

Figure S4. Curie–Weiss fit (red solid line) of the inverse magnetic susceptibility $1/\chi_M$ for **2**